Catalysis Letters (2021) 151:1882–1893
https://doi.org/10.1007/s10562-020-03445-z

Fabrication of Nitrogen-Enriched Graphene Oxide on the DFNS/Metal NPs as a Nanocatalysts for the Reduction of 4-Nitrophenol and 2-Nitroaniline

Zhiyong Shao[1] · Seyed Mohsen Sadeghzadeh[2]

Received: 5 August 2020 / Accepted: 28 October 2020 / Published online: 5 November 2020

Abstract
DFNS is functionalized by using graphene oxide (GO) (*N*-enriched GO) as a robust anchor. Hence, the metal nanoparticles (NPs) are well-dispersed without aggregation over the DFNS/GO (DFNS/GO/X, X = Pd, Au, Cu). For preventing the restacking of graphene sheets, the supramolecular polymerized GO behaves not only as a spacer but also as a nitrogen source for producing active centers in the case of metal NP attachments. In this way, the nitrogen over the level of the GO sheets adjusts with copper ions in order to synthesis palladium nanoparticles. Water pollution is known as a significant global concern that can threat the entire biosphere and can influence the lives of many millions of people in the world. Water pollution can make many diseases and millions of people die annually due to illness caused by the dirty water. 4-nitrophenol and also 2-nitroaniline, which have been specified as hazardous toxic. In addition, wastes contaminants are in USEPA's list. Therefore, developing novel approaches are essential in order to eliminate these waste contaminants. In the case of the synthesize of colors and drugs, powerful performers o-phenylenediamine (o-PDA) and powerful performers were intended as considerable intermediate that preparation from 2-NA as well as 4-NP. As-prepared DFNS/GO/X (X = Pd, Au, Cu) nanostructures are used for the 4-nitrophenol and 2-nitroaniline reduction that causing high efficiency of the reaction by taking into account of chemoselectivity.

✉ Zhiyong Shao
shao6585@sina.com

✉ Seyed Mohsen Sadeghzadeh
seyedmohsen.sadeghzadeh@gmail.com

[1] State Key Laboratory of Biobased Material and Green Papermaking, Qilu University of Technology, Shandong Academy of Sciences, Jinan 250353, China

[2] Department of Chemistry, Faculty of Sciences, Neyshabur Branch, Islamic Azad University, Neyshabur, Iran

Graphic Abstract

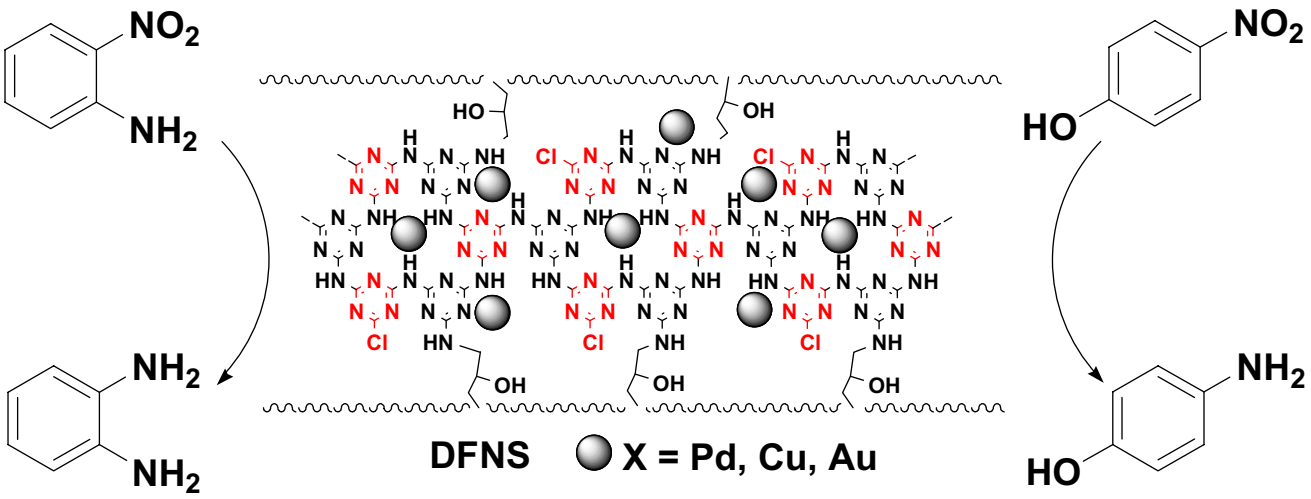

Keywords Nano catalyst · Graphene oxide · Green chemistry · 4-Nitrophenol

1 Introduction

Recently, to reduce environmental pollution coming from the world population, green chemistry is introduced as an excellent approach [1–7]. In aqueous solution, to transfer organic debris in reusable mixtures using less toxic, methods pass taking of harmful organic solvents have been highly investigate by scholars. They have focused on the accessibility of nitroaromatic materials. In industrial and also agricultural waste water, high concentration of Nitrophenols can be found that are the most common organic pollutants specified [8, 9]. Nitrophenols in their low concentrations in a constant amount of water is harmful for the health of us and aquatic life because of potential mutagenic and carcinogenic influences of Nitrophenols [10, 11]. Hence, 2-nitroaniline together with 4-nitrophenol are perilous wastes known as toxic pollutions [12–16]. Therefore, developing novel approaches are essential in order to eliminate these risk. Moreover, for making colors and drugs, which produce by from 4-NP and 2-NA, 4-aminophenol (4-AP), and o-phenylenediamine (o-PDA) are important intermediate [17–21].

In the catalytic zone, noble metal nanoparticle (NMNPs) based heterogeneous catalysts have been widely studied due to the high catalytic efficiency in different liquid-phase catalytic approaches [22, 23]. Exclusively, metal NPs based catalysts were highly regarded by researchers due to the promising catalytic efficiency in the cases of diverse reactions such as the Heck C–C coupling [24], Suzuki coupling [25, 26], hydrogenation [27], degradation of fuel cells [28] and pollutants [29]. The catalytic activity of metal NPs is corresponded to the active atoms onto the level that are usually corresponded to the attributes of level [30]. However, smaller metal NPs proved high catalytic activity because of existing a higher surface-to-volume ratio [31, 32]. The surface energy of the metal NPs can be improved by decreasing the size of metal NPs leading to the trend of interparticle aggregation, which can be associated with the

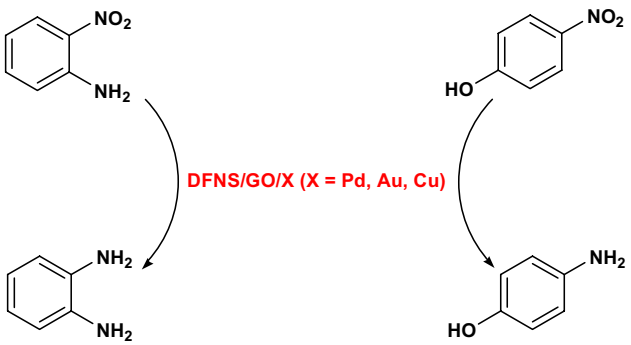

Scheme 1 Reduction of 4-NP and 2-NA of alkylphenols at the presence of DFNS/GO/X (X = Pd, Au, Cu) NPs

catalytic efficiency [33]. Nevertheless, the stability of Pd NPs is another impressive issue for their application. For metal NP stabilization, the utilizing proper support materials can be a good option. Carbon [34, 35], Al_2O_3 [36, 37], mesoporous silica [38] and core–shell magnetic mesopores [39] as supports are utilized for the immobilization of Pd NPs because of their robust surface chemistry and excellent high surface areas and also stability. Upper mentioned materials have large specific surface areas leading to the great dispersion of the NPs. Hence they can barricade the NPs aggregation and enhance the activity of the catalyst system. Nevertheless, the low accessibility to the active sites leads to a reduction of the influence of mass transfer for all of the mentioned catalysts. Silica supports have appropriate feedbacks because of having easily accessible high surface areas. Recently, using surfactant on soft templating is led to the production of mesoporous silica with dendrimetic silica fibers morphology (DFNS). For adsorption and catalysis applications as support material, silica having this morphology is evaluated. In terms of reactants, the outward radial widening of these silicas possesses higher surface area to enhance the functional materials. In addition, DFNS has intrinsic mesoporous properties, thermally stable and high activity. The DFNS production requires microemulsion system that involves oil, surfactant, and water. Moreover, the particle size and morphology of DFNS were manipulated by utilizing co-surfactant and many co-solvents [40–47].

Graphene (GO) solid supports include a 2D (two-dimensional) structure and have abundant oxygen-containing functional groups like carboxylic acid, hydroxyl, and hydroxyl epoxy groups [48–53] that is aggregated due to the strong π–π stacking as well as van der Waals interaction that occurred among GO sheets. It can cause the loss of active levels for catalytic usages. In contrast, more structural enhancing of GO using heteroatom-enrichment, such as nitrogen-enrichment, enhance active levels over the GO surface, significantly. Many techniques like magnetron laser ablation [54] and sputtering [55] as well as chemical vapor deposition of nitrogen-containing organic precursors [56] are proposed to produce nitrogen-enriched carbon materials. Nevertheless, the upper mentioned techniques are rather costly, complex and not easily amenable to scale-up purpose. Particularly, whole products are achieved at the high-temperature more than 500 °C. In this way, the synthesize of DFNS/GO/X (X = Pd, Au, Cu) is performed and investigated. In addition, the application of nanocatalyst to catalytic reduction of 4-NP and 2-NA (Scheme 1).

2 Experimental

2.1 Materials and Methods

Chemical materials are provided from Merck and Fluka in high purity. In an open capillaries, using an Electrothermal 9100 apparatus, melting points are specified. FTIR spectra are identified on a spectrometer of VERTEX 70 (Bruker) in the transmission modein spectroscopic grade KBr pellets in the case of all the powders. The structure and particle size of nano particle is demonstrated utilizing a Philips CM10 transmission electron microscope operating at 100 KV. Powder X-ray diffraction data are achieved by Bruker D8 Advance model along with Cu ka radition. The thermogravimetric analysis (TGA) is done on a NETZSCH STA449F3 at a heating rate of 10 °C min^{-1} under nitrogen. ^{1}H and ^{13}C NMR spectra are obtained on a spectrometer of BRUKER DRX-300 AVANCE at 300.13 and 75.46 MHz, spectrometer of BRUKER DRX-400 AVANCE at 400.22 and 100.63 MHz, respectively. For C, N, and H, elemental evaluations are done by a Heraeus CHN–O-Rapid analyzer. The purity of the products and reaction analyzing are performed using TLC on plates of silica gel polygram SILG/UV 254. Mass spectra are specified by Shimadzu GCMS-QP5050 Mass Spectrometer.

2.2 Total Approach for the Preparation of DFNS NPs

2.5 g of TEOS is released in a solution of 30 mL cyclohexane and 1.5 mL 1-pentanol. After that, a stirred solution of urea (0.6 g) along with cetylpyridinium bromide (CPB 1 g) in water (30 mL) is added. The obtaining mixture is stirred, continually, for 45 min under the temperature of 25 °C and placed in a teflon-sealed hydrothermal reactor and was heated at 120 °C for 5 h. Then, the silica obtained is isolated using centrifugation, washed by acetone and deionized water (DI), and dried using a drying oven. This material is calcined under the temperature of 550 °C for 5 h in air [46].

2.3 Total Approach for the Preparation of DFNS/GMSI NPs

A mixture is obtained by mixing a constant amount of DFNS (200 mg) in THF (20 ml) followed by the addition of NaH (20 mmol) through ultrasonication. Then, 22 mmol of (3-glycidyloxypropyl)trimethoxysilane are added released in the mixture under the temperature of

25 °C and stirred for 16 h at 50 °C. The resulted mixture is filtered and then washed by DI and ethanol. After that, the filtered solids are dried in vacuum condition under the temperature of 50 °C for 3 h [46].

2.4 Total Approach for the Preparation of DFNS/GO NPs

100 mg of DFNS that is activated by glycidyloxypropyl released in 10 mL of acetate buffer (0.1 M and pH 4.5) including a constant amount of graphene oxide (50 mg, GO). For obtaining nanoparticles (NPs) containing PEI, the suspension is shaken at 120 rpm speed for a few hours. The obtained NPs are washed many times and stored at 4 °C by utilizing acetate buffer.

2.5 Total Approach for the Preparation of DFNS/GO/Au NPs

Structures of DFNS/GO/Au NPs are provided with reaction of DFNS/GO NPs with $HAuCl_4{\cdot}3H_2O$. First, for ensuring adequate adsorption of $HAuCl_4{\cdot}3H_2O$ by the DFNS/GO NPs 0.05 g of DFNS/GO NPs is dispersed in 5 cm^{-1} of a 0.1 M gold precursor solution of ($HAuCl_4{\cdot}3H_2O$; 99.99%; Aldrich) and then the solution was stirred by a mechanical stirrer for 1.5 h. after that, the catalyst of DFNS/GO/Au NPs are obtained using filtration and washed by ethanol and DI.

2.6 Total Approach for the Preparation of DFNS/GO/Pd NPs

A round-bottom flask equal to 100 mL is charged by DFNS/GO nanocomposite (0.5 g) and 0.1 g of $Pd(OAc)_2$ as well as acetonitrile (50 mL), after that it is dispersed, ultrasonically, for 30 min. In the following, the fresh solution of $NaBH_4$ (0.2 M, 10 mL) is added dropwise in the uppermetnrioned suspension. The product is isolated with centrifugation, washed frequently by DI and ethanol, and dried in a vacuum.

2.7 Total Approach for the Preparation of DFNS/GO/Cu NPs

0.5 g of DFNS/GO NPs is dispersed in 50 mL of H_2O, ultrasonically, and subsequently $CuCl_2{\cdot}2H_2O$ (0.1 g) is released in solution. Excess amount of $NaBH_4$ solution was added dropwise after being stirred for around a half of hour. After that, the Cu NPs are obtained and anchored over the DFNS/GO NPs. Therefore, the nanocatalyst of DFNS/GO/Cu NPs is provided by centrifugation and in the last step, it was dried invacuum.

2.8 General Approach for the Reduction of 4-Nitrophenol

In the first step, 30 µL of aqueous 4-NP solution (1.25×10^{-2} mol/L) is released in water (2.0 mL). After that, it is mixed by 0.1 mL of freshly prepared aqueous $NaBH_4$ solution (0.4 M) and a deep yellow solution was achieved.

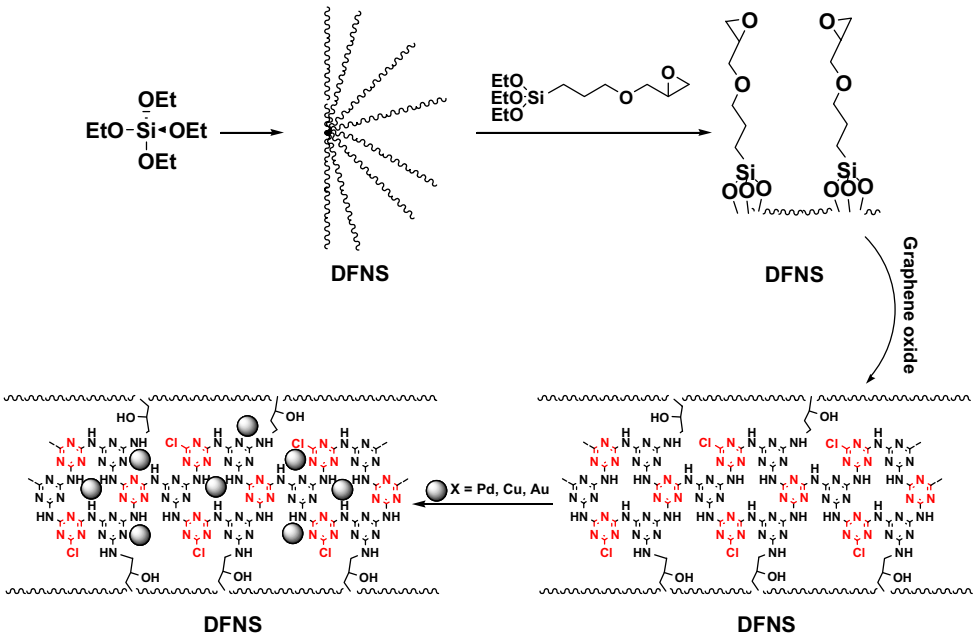

Scheme 2 A schematic illustration of the preparation of DFNS/GO/X (X = Pd, Au, Cu) nanocatalyst

DFNS/GO/X (X = Pd, Au, Cu) (0.5 mg) was added to the

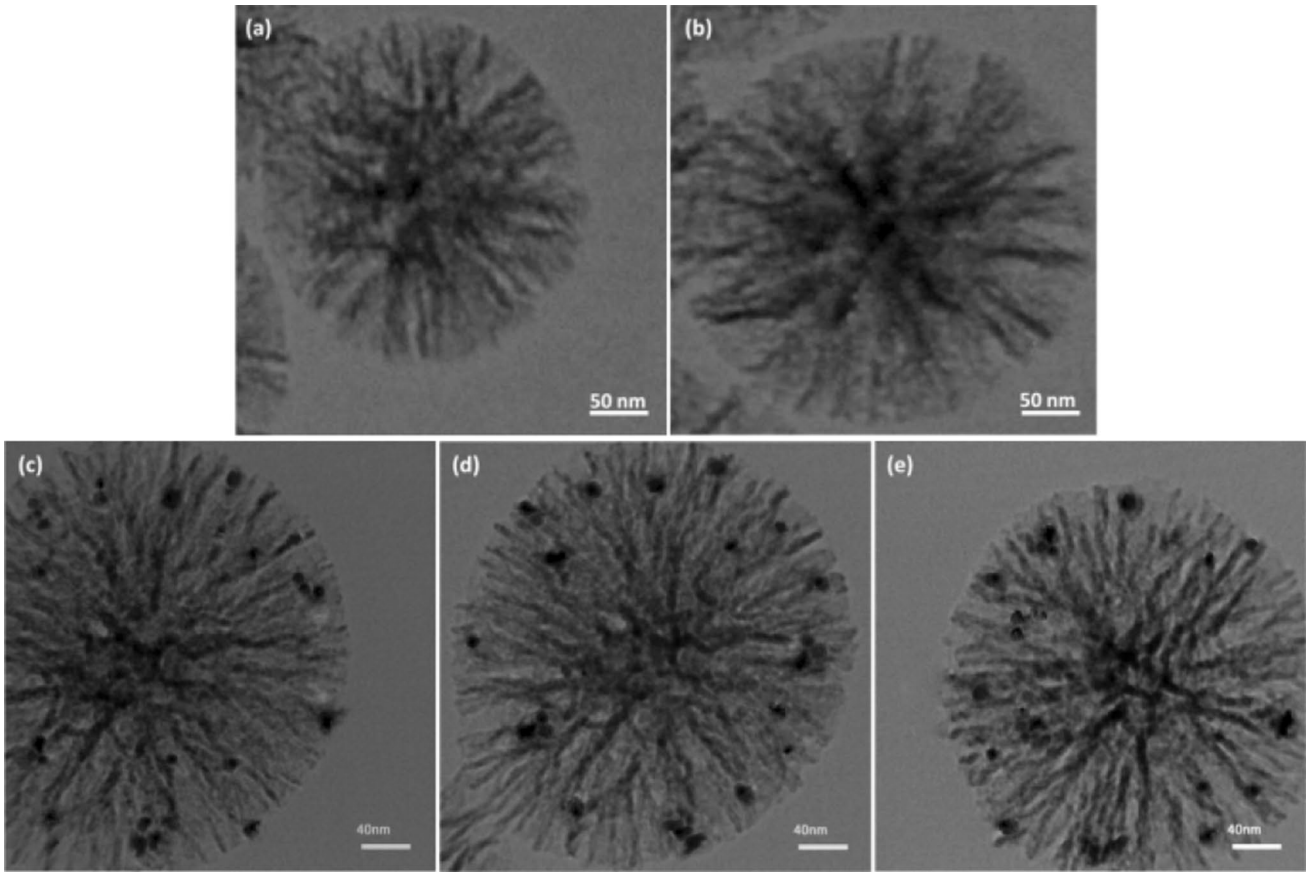

Fig. 1 TEM images of DFNS (**a**), DFNS/GO (**b**), DFNS/GO/Cu (**c**), DFNS/GO/Au (**d**), and DFNS/GO/Pd (**e**)

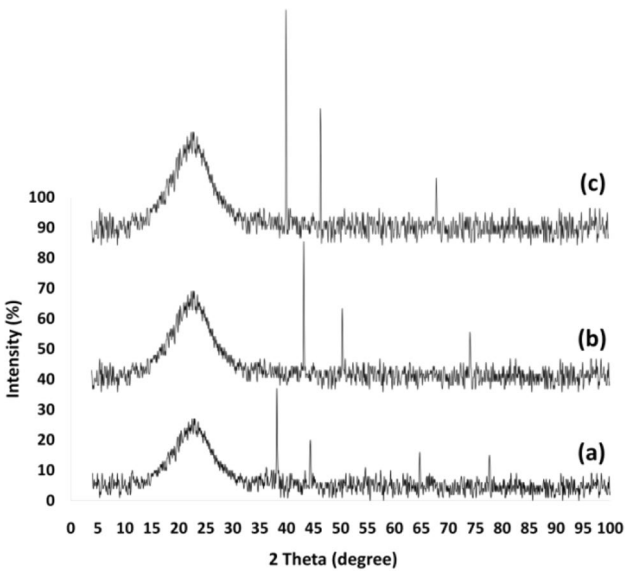

Fig. 2 Powder XRD patterns of DFNS/GO/Au (*a*), DFNS/GO/Cu (*b*), and DFNS/GO/Pd (*c*)

yellow solution. After that, the reaction is completed while the solution became colorless. The progress of reaction was analyzed utilizing UV–Vis absorption spectra for the reaction mixture.

2.9 General Method for the Reduction of 2-Nitroaniline

DFNS/GO/X (X = Pd, Au, Cu) (0.5 mg) was added in water (2.0 mL), and then mixed by 0.1 mL of $NaBH_4$ (0.4 M) solution and 2-NA aqueous solution (30 μL, 1.25×10^{-2} mol/L) was quickly injected with stirring. The mixture color considerably vanished, indicating the reduction of 2-NA. The reaction trend is analyzed with calculating the UV-vis absorption spectra of the reaction mixture.

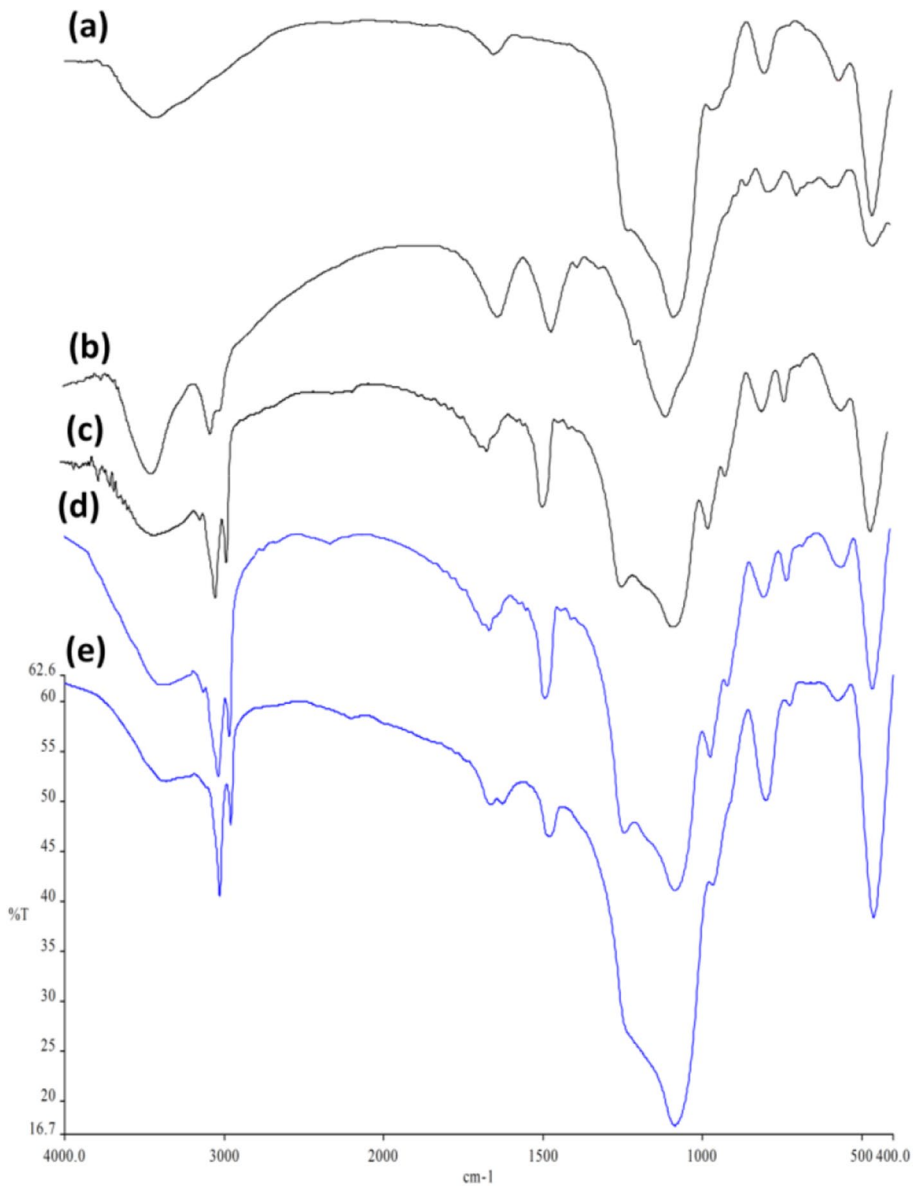

Fig. 3 FT-IR spectra of DFNS (*a*), DFNS/GO (*b*), DFNS/GO/Pd (*c*), DFNS/GO/Cu (*d*), and DFNS/GO/Au (*e*)

Table 1 The loading amount of Cu, Au, and Pd in DFNS/GO/X and DFNS/X

Entry	Catalyst	Wt%
1	DFNS/GO/Cu	3.4
2	DFNS/GO/Au	3.2
3	DFNS/GO/Pd	3.6
4	DFNS/Cu	2.0
5	DFNS/Au	1.9
6	DFNS/Pd	2.2

3 Results and Discussion

In the present study, GO is synthesized and modified by taking into consideration of in situ fabrication of nitrogen-enriched GO utilizing a supramolecular polymerization reaction among cyanuric chloride and melamine under temperature lower than 120 °C. This process is introduced as a catalyst support due to significant advantages like thermal and chemical stability, being inexpensive easy and easy for preparing and having much more active sites in comparison to GO. After that, metal nanoparticles are immobilized over the DFNS/GO surface (Scheme 2).

The TEM images for the catalysts of DFNS, DFNS/GO, and DFNS/GO/X (X = Au, Pd, Cu) are illustrated in Fig. 1. As observed in Fig. 1a, the DFNS NPs possessed a firm particle size in the range of 200–250 nm. For forming DFNS/GO core-shell particles polymerized graphene oxide is coated over the DFNS (Fig. 1b). In addition, the metal NPs were distinguishable, clearly, due to the difference in their contrast after anchoring of Au, Pd, and Cu. It is observed

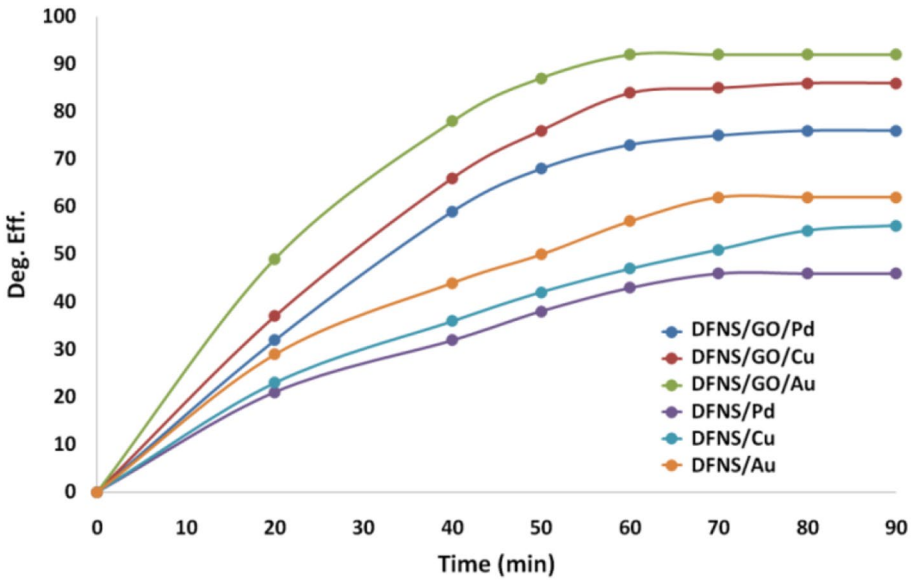

Fig. 4 Effect of time on yield of the reduction of 4-NP

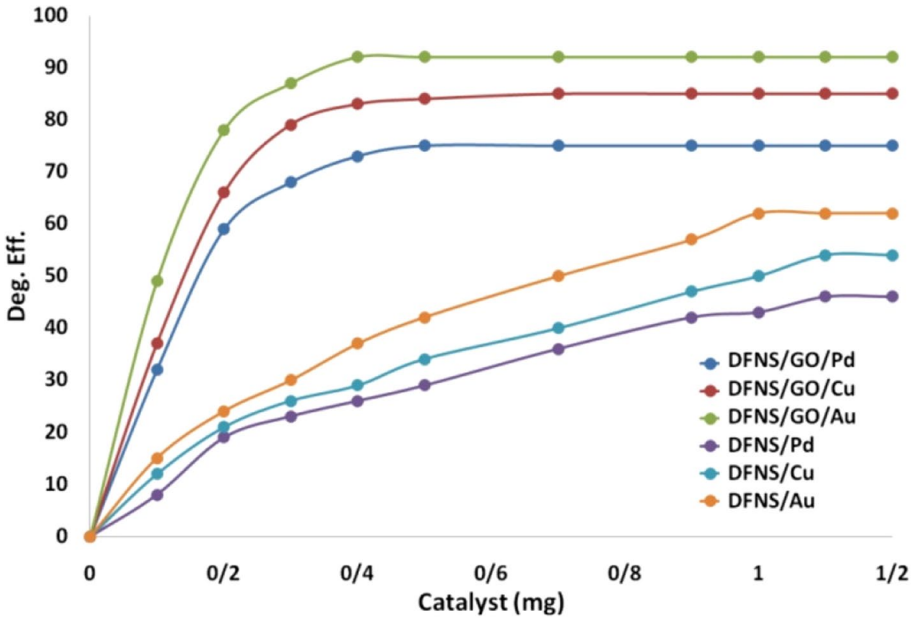

Fig. 5 Effect of the amount of catalyst on yield of the reduction of 4-NP

that the as-prepared metal NPs are spherical without considerable aggregation (refer to Fig. 1c–e).

To achieve more information in the case of their crystallographic attributes and molecule structures Patterns of X-ray diffraction as well as the infrared spectra of DFNS/GO/X (X = Au, Pd, Cu) NPs are measured. Figure 2 shows the XRD patterns for DFNS NPs, and as-prepared DFNS/GO/X (X = Au, Pd, Cu) NPs catalyst. The broad peak between 20 and 30° relates to amorphous silica. Figure 2a shows new peaks at 2θ = 38.2°, 44.4°, 64.6° and 77.6° that are reflection of Au (JCPDS 04-0784), 2θ = 43.3°, 50.4°. Moreover, peak at 74.1° is reflection of Cu (JCPDS No. 04-0836) (refer to Fig. 2b), and 2θ = 40.1°, 46.5° and 68° are reflection of Pd (JCPDS 05-0681) crystal, as seen in Fig. 2c, are seen for DFNS/GO/Au, DFNS/GO/Cu, and DFNS/GO/Pd, respectively. These figures confirmed the appropriate growth of metal particles over the level of DFNS/GO again.

The reactions are analyzed by using FTIR (Fig. 3). The band at 1090 cm^{-1} is considered to the vibration of the Si-O bonds for unmodified DFNS (Fig. 3a). Two bands at 3012 and 2982 cm^{-1} along with C-H stretching considerably increased after the polymerized GO on the surface of DFNS. However, Fig. 3b shows two new bands at 1571 and 1488 cm^{-1} along with C-C and C-H stretching, respectively. It is observed that the IR spectrum of the catalyst of DFNS/GO/X (X = Cu, Pd, Au) proves that nearly no variation occurs after immobilization of Au, Pd, and Cu over the DFNS/GO level (refer to Fig. 3c–e), however, the metal NPs

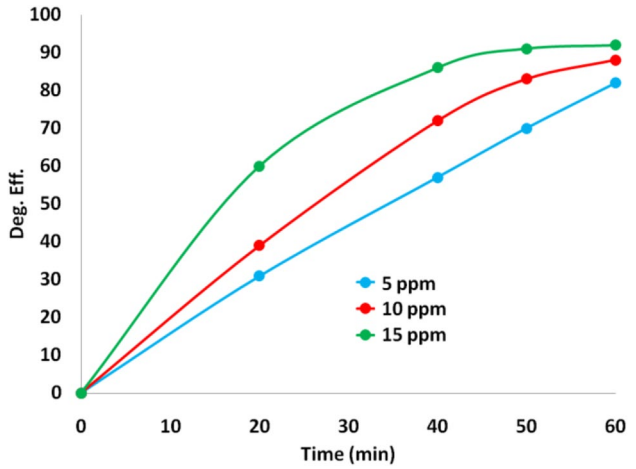

Fig. 6 The effect of concentration of 4-nitrophenol on the reduction efficiency. *a* 5 ppm, *b* 10 ppm, *c* 15 ppm

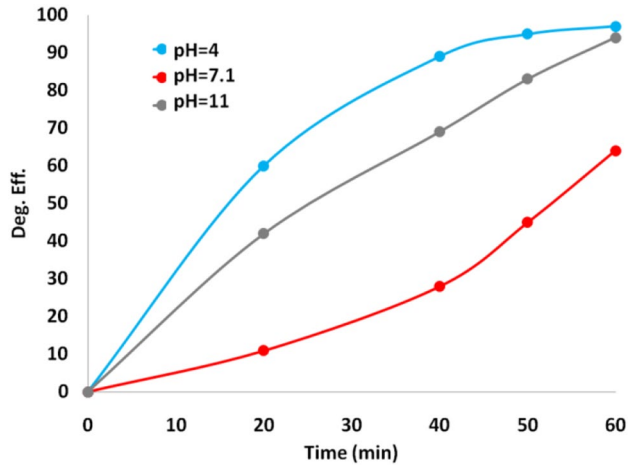

Fig. 7 The effect of pH on the reduction yield by using 4-NP and DFNS/GO/Au as catalyst

Table 2 Influence of different catalysts on the reduction of 4-NP

Entry	Catalyst	Yield (%)[a]
1	DFNS	–
2	DFNS/GO	–
3	X (X = Au, Pd, Cu)	
	Au	90
	Pd	69
	Cu	83
4	KCC-1/GO/X (X = Au, Pd, Cu)	
	Au	92
	Pd	73
	Cu	84

[a]Isolated yield

is dispersed over the DFNS/GO level from the TEM image for the DFNS/GO/X.

The DFNS/GO/X (X = Au, Pd, Cu) is compared to DFNS/X (X = Au, Pd, Cu) in order to investigate the exact influence of using GO in the catalyst. The loading value in the case of Cu, Au, and Pd in DFNS/GO/X as well as DFNS/X specified by inductively coupled plasma mass spectrometry (ICP-MS). The motionless nanoparticle amount in DFNS/GO/X is around twice DFNS/X. Comparing mentioned amounts, proved appropriate efficiency of GO (refer to Table 1).

The reduction of 4-NP in 4-AP under the existence of $NaBH_4$ is utilizedas a novel model, and is done considering different reaction factors like time and amount of the catalyst to optimize the reaction states and achieve the most appropriate catalytic activity. In this paper, it is determined that in 60 min and at the attendance of 0.5 mg, DFNS/GO/X (X = Au, Pd, Cu) has better efficiency, considering reaction time and the reduction of 4-NP yield. However, it is in the attendance of 1.0 mg DFNS/ X (X = Au, Pd, Cu) 80 min. Figures 4 and 5 shows the view the terms easier to reaction at the attendance of GO, proof of its efficiency.

The reduction of 4-NP, 5, 10, and 15 ppm was investigated. A constant amount of 4-NP (92%) is declined in 1 h of irradiation while the concentration is 5 ppm. Reduction efficiency reduced to 88% considering the same irradiation time by enhancing the organic pollution concentration to 10 ppm. Figure 6 shows that product reduces 82% of 4-nitrophenol while the concentration is 15 ppm.

The effects of pH on the yield of reduction is investigated utilizing 4-NP. Figure 7 shows outcomes in the case of reduction of 4-NP by DFNS/GO/Au in acidic (pH = 4), neutral (pH = 7.1), and basic condition. 97% of 4-NP is reduced for pH of 4 utilizing HNO_3. In neutral pH (pH 7.1) percentage of reduction is 64%, while about 94% of 4-NP is reduced in basic pH of 11. Explaining the influences of pH on the dye photoreduction efficiency is a tough task due to its multiple duties. Highest efficiency of reduction is obtained at acidic pH. It occurs due to strong adsorption of the reduction over the DFNS/GO/Au species obtained from the electrostatic attraction of the positively varied DFNS/GO/Au by the negatively charged dye. Moreover, higher reduction efficiency can be obtained at basic pH in comparison to the neutral pH. It can be due to the fact that formation of hydroxyl radicals can be properly performed at basic pH levels. Hydroxyl radicals formed from the reaction among positive holes and hydroxide ions (refer to Fig. 7).

Different control experiments are done and the obtained data for evaluating the efficiency of the catalyst, as seen in Table 2. Lastly, two separated reactions are evaluated at the attendance of DFNS along with DFNS/GO. The obtained outcomes proved that any reduction of 4-NP is not seen (refer to Table 2, entries 1 and 2). The research

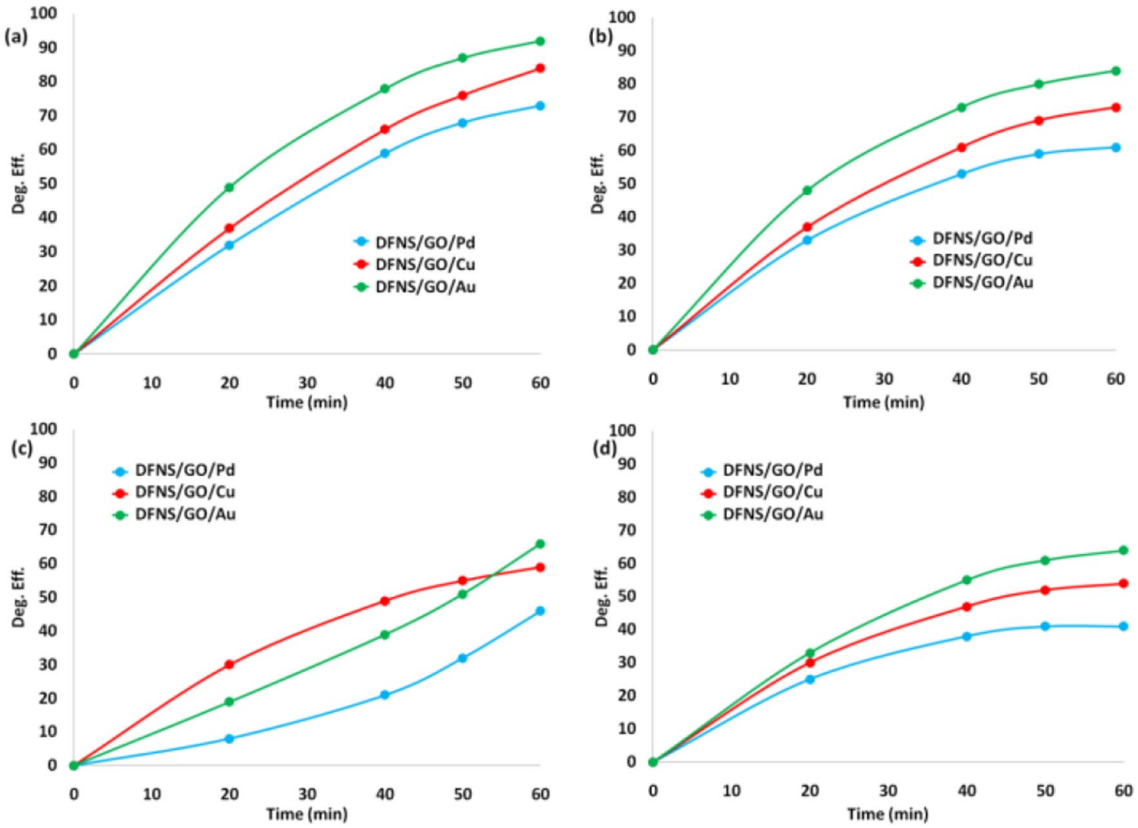

Fig. 8 Photocatalysis results for the reduction of (**a**) 4-nitrophenol, (**b**) 2-nitroaniline, (**c**) nitrobenzene, and (**d**) 1-(4-nitrophenyl)ethanone by using DFNS/GO/X (X = Au, Pd, Cu). In order to study the effect of pollution concentration on reduction efficiency, DFNS/GO/Au was used as the most efficient photocatalyst

Table 3 Analysis the amount of Au, Pd, and Cu from DFNS/GO/X and DFNS/X

Entry	Metal (X)		ppm
1	DFNS/GO/X	Au	0.2
		Pd	0.3
		Cu	0.2
2	DFNS/X	Au	1.2
		Pd	0.9
		Cu	0.8

was continued for improving the yield of the reaction with the optimization of the reaction states according to these frustrating outcomes. In addition, the reaction was smoothly performed by the use of DFNS/GO/X (X = Au, Pd, Cu) as well as X = Au, Pd, Cu as the catalyst, and the DFNS/GO/X (X = Au, Pd, Cu) is detected more effective compared to X = Au, Pd, Cu (Table 2, entries 3 and 4). It is determined that DFNS/GO/X (X = Au, Pd, Cu) is utilized in the subsequent studies due to its high reactivity, easy separation, and high selectivity.

The photocatalytic activity of DFNS/GO/X nanostructure is investigated considering the reduction of 4-nitrophenol, 2-nitroaniline, nitrobenzene, and 1-(4-nitrophenyl) ethanone by UV light for 60 min. The reduction efficiency of mentioned dyes utilizing the catalyst of DFNS/GO/X NPs under UV light for 60 min is shown in Fig. 10. Photocatalyst evaluation is performed in neutral pH and 5 ppm dye concentration. As seen in Fig. 8a, reduction efficiency for DFNS/GO/Au, DFNS/GO/Pd, and DFNS/GO/Cu and 4-nitrophenol is 92, 73, and 84%, respectively. The lowest photocatalytic activity is obtained when DFNS/GO/Pd is used as the catalyst. However, DFNS/GO/Au as surfactant demonstrates the maximum reduction efficiency for radiation of 1 h. Figure 8b shows that the same recipe is utilized for studying the reduction of 2-nitroaniline. DFNS/GO/Pd reduces 61% of 2-nitroaniline under 1 h radiation. Reduction efficiency enhanced to 73% by varying the photocatalyst to DFNS/GO/Cu. By varying surfactant to DFNS/GO/Au, for removal of 2-nitroaniline, the highest removal efficiency is obtained. Figure 8c shows the yield of reduction for nitrobenzene. DFNS/GO/Au, DFNS/GO/Pd, and DFNS/GO/Cu degrade 66, 46, and 59%, of nitrobenzene under UV radiation for 1 h, respectively. In the last step, 1-(4-nitrophenyl)ethanone is utilized as organic pollution by concentration of 5 ppm, as can be seen in Fig. 8d. DFNS/GO/Au indicates the highest photocatalytic activity.

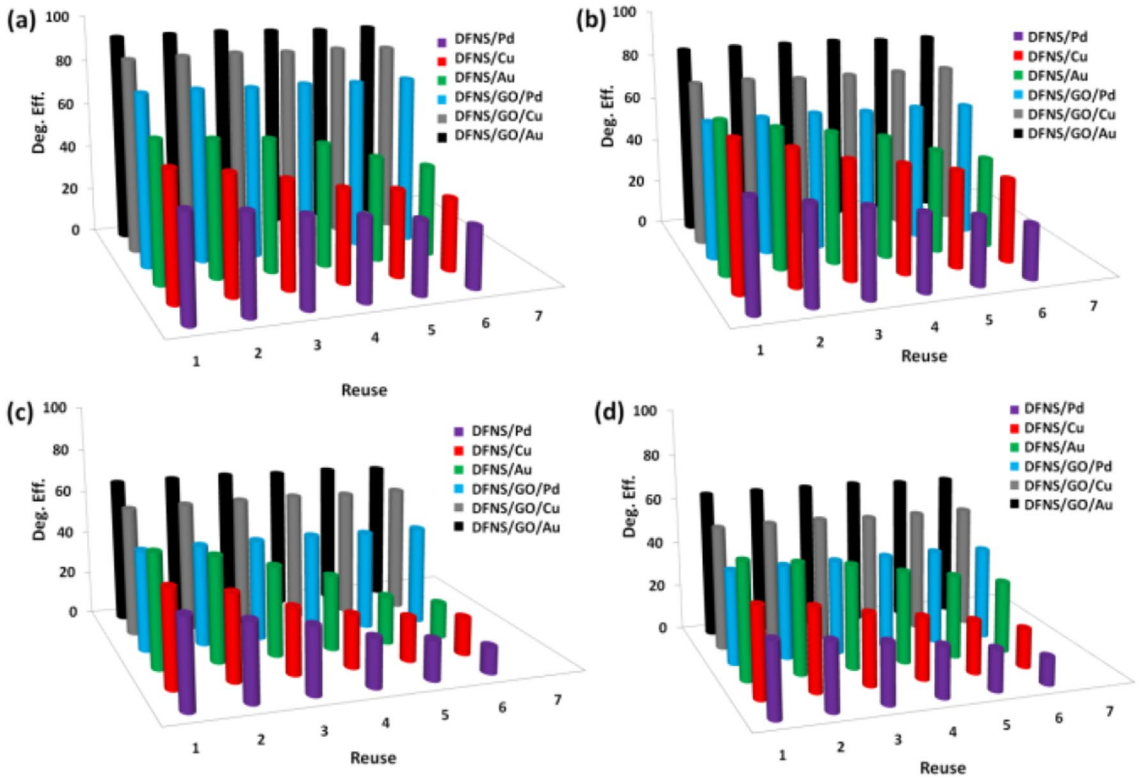

Fig. 9 Reuses performance of the catalysts for the reduction of (**a**) 4-nitrophenol, (**b**) 2-nitroaniline, (**c**) nitrobenzene, and (**d**) 1-(4-nitrophenyl) ethanone by using DFNS/GO/X (X = Au, Pd, Cu) and DFNS/X (X = Au, Pd, Cu)

It declines 64% of 1-(4-nitrophenyl)ethanone after 60 min. It is specified that utilizing DFNS/GO/Au as catalyst cause enhancing photocatalytic activity.

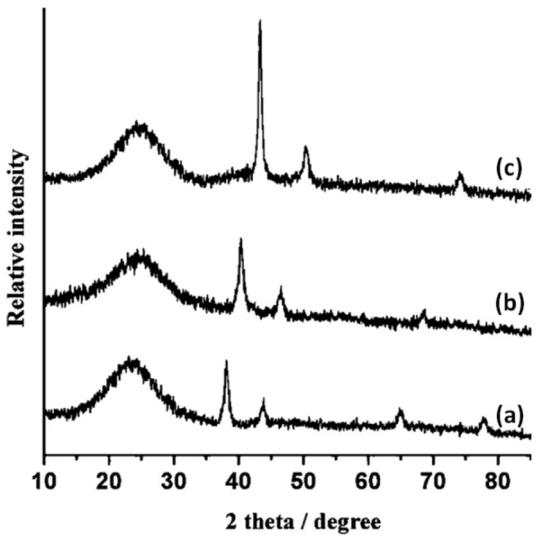

Fig. 10 Powder XRD patterns of recovered DFNS/GO/Au (*a*), DFNS/GO/Pd (*b*), and DFNS/GO/Cu (*c*)

The model reaction of reduction of 4-nitrophenol was carried out under the optimized conditions for verifying whether or not the catalysis is actually heterogeneous or is because of existing many leached active species in the liquid phase, and the catalyst is separated by taking into account of filtration from the reaction mixture. The analysis of coupled plasma mass spectrometry (ICP-MS) demonstrated that the amount of Cu, Au, and Pd from DFNS/GO/X leaching in the mixture of reaction is very low. However, it was much more amount in the case of DFNS/X, considerably. This proves the high performance of GO (refer to Table 3).

The obtained outcomes showed that the catalysts are stable and can to lerate the present reaction states. The recyclability of catalysts is evaluated by the model of reaction considering the same conditions. From the reaction mixture, the catalysts are recovered by filtration after the required time and then washed by ethyl acetate, and dried under the temperature of 100 °C and reused. DFNS/GO/X NPs presented almost same catalytic activity after ten consecutive reuses, but it is not for DFNS/X NPs, as seen in Fig. 9. This difference in yield is due to the fact that it is constructed and produced GO-functionalized DFNS.

Finally, after the passage of the 6th of catalytic reduction for 4-nitrophenol at the specified premium conditions by some study in order to ensure whether the structure of the

recovered catalyst is maintained (Fig. 10). Figure 10 shows XRD pattern for the reproduced catalyst. It demonstrated that the structure of catalyst remained completely intact in recycling. Noted that, the nanocatalyst did not illustrate any morphological variations.

4 Conclusions

In this paper, for the first time, a new kind of robust catalytic hybrids according to the hyperbranched graphene oxide-functionalized DFNS and utilized it as noble metal nanocatalyst supports. Many noble metal nanocatalysts like Cu, Au, and Pd can be grown, immediately, over the DFNS surface firmly with monodisperse size and ultrasmall, high loading capacity, and uniform distribution due to the unique structure and many functional groups of GO. As prepared DFNS/GO/X nanostructures are utilized for treating water contain 4-nitrophenol, 2-nitroaniline, nitrobenzene, and 1-(4-nitrophenyl)ethanone. Moreover, the concentration effect of contaminant as well as its pH over the reduction efficiency are investigated. Nanostructures of DFNS/GO/X demonstrate higher photocatalytic activity in an acidic environment and also lower concentration of contaminant. The DFNS/GO/X (X = Au, Pd, Cu) compared with DFNS/X (X = Au, Pd, Cu) for assessing the exact influence of the attendance of GO in the catalyst. The motionless nano particle amount existing in DFNS/GO/X is around twice DFNS/X. Form comparing these data, the GO efficiency is proved.

Acknowledgements The Project Supported by the Foundation (No. ZR20190106) of State Key Laboratory of Biobased Material and Green Papermaking, Qilu University of Technology, Shandong Academy of Sciences.

Compliance with Ethical Standards

Conflict of interest The authors declare that they have no conflict of interest.

References

1. Zhang J, Chen G, Chaker M, Rosei F, Ma D (2013) Appl Catal B Environ 132:107–115
2. Cardenas-Lizana F, Lamey D, Perret N, Gomez-Quero S, Kiwi-Minsker L, Keane MA (2012) Catal Commun 21:46–51
3. Sadeghzadeh SM, Zhiani R, Emrani S (2018) Catal Lett 148:119–124
4. Zarejousheghani M, Moeder M, Borsdorf H (2013) Anal Chim Acta 798:48–55
5. Li X, Wang X, Song S, Liu D, Zhang H (2012) Chem Eur J 18:7601–7607
6. Coccia F, Tonucci L, Bosco D, Bressan M, d'Alessandrro N (2012) Green Chem 14:1073–1078
7. Yoosefian M, Mola A, Fooladi E, Ahmadzadeh S (2017) J Mol Liq 225:34–41
8. Etminan N, Yoosefian M, Raissi H, Hakimi M (2016) J Mol Liq 214:313–318
9. Yoosefian M (2017) Appl Surf Sci 392:225–230
10. Le X, Dong Z, Zhang W, Li X, Ma J (2014) J Mol Catal A Chem 395:58–65
11. Le X, Dong Z, Li X, Zhang W, Le M, Ma J (2015) Catal Commun 59:21–25
12. O'Connor OA, Young LY (1989) Environ Toxicol Chem 8:853–862
13. Oturan MA, Peiroten J, Chartrin P, Acher AJ (2000) Environ Sci Technol 34:3474–3479
14. Li K, Zheng Z, Huang X, Zhao G, Feng J, Zhang J (2009) J Hazard Mater 166:213–220
15. Zhang Y, Yuan X, Wang Y, Chen Y (2012) J Mater Chem 22:7245–7251
16. Saha S, Pal A, Kundu S, Basu S, Pal T (2010) Langmuir 26:2885–2893
17. Sahiner N, Karakoyun N, Alpaslan D, Aktas N (2013) Int J Polym Mater Polym Biomater 62:590–595
18. Yang Y, Guo Y, Liu F, Yuan X, Guo Y, Zhang S, Guo W, Huo M (2013) Appl Catal B Environ 142–143:828–837
19. Mohamed MM, Al-Sharif MS (2013) Appl Catal B Environ 142–143:432–441
20. Muniz-Miranda M (2014) Appl Catal B Environ 146:147–150
21. Ozay H, Kubilay S, Aktas N, Sahiner N (2011) Int J Polym Mater 60:163–173
22. Paganelli S, Piccolo O, Baldi F, Tassini R, Gallo M, La Sorella G (2013) Appl Catal A 451:144–152
23. Shiraishi Y, Fujiwara K, Sugano Y, Ichikawa S, Hirai T (2013) ACS Catal 3:312–320
24. Imamura K, Yoshikawa T, Nakanishi K, Hashimoto K, Kominami H (2013) Chem Commun 49:10911–10913
25. Le X, Dong Z, Jin Z, Wang Q, Ma J (2014) Catal Commun 53:47–52
26. Wang P, Liu H, Niu J, Li R, Ma J (2014) Cat Sci Technol 4:1333–1339
27. Zhang F, Jin J, Zhong X, Li S, Niu J, Li R, Ma J (2011) Green Chem 13:1238–1243
28. Dong Z, Le X, Dong C, Zhang W, Li X, Ma J (2015) Appl Catal B 162:372–380
29. Yang MQ, Pan X, Zhang N, Xu YJ (2013) CrystEngComm 15:6819–6828
30. Antolini E (2009) Energy Environ Sci 2:915–931
31. Lee H, Habas SE, Kweskin S, Butcher D, Somorjai GA, Yang P (2006) Angew Chem Int Ed 45:7824–7828
32. Zeng J, Zhang Q, Chen J, Xia Y (2009) Nano Lett 10:30–35
33. Lin Y, Qiao Y, Wang Y, Yan Y, Huang J (2012) J Mater Chem 22:18314–18320
34. Yuan G, Keane MA (2007) Ind Eng Chem Res 46:705–715
35. Wei S, Ma Z, Wang P, Dong Z, Ma J (2013) J Mol Catal A Chem 370:175–181
36. Fang Y, Wang E (2013) Nanoscale 5:1843–1848
37. Ganapathy D, Sekar G (2013) Catal Commun 39:50–54
38. Polshettiwar V, Cha D, Zhang X, Basset JM (2010) Angew Chem 49:9652–9656
39. Li W, Zhang B, Li X, Zhang H, Zhang Q (2013) Appl Catal A 459:65–72
40. Maity A, Polshettiwar V (2017) ChemSusChem 10:3866–3913
41. Kundu PK, Dhiman M, Modak A, Chowdhury A (2016) ChemPlusChem 81:1142–1146
42. Gautam P, Dhiman M, Polshettiwar V, Bhanage BM (2016) Green Chem 18:5890–5899
43. Fihri A, Cha D, Bouhrara M, Almana N, Polshettiwar V (2012) ChemSusChem 5:85–89

44. Sadeghzadeh SM, Daneshfar F, Malekzadeh M (2014) Chin J Chem 32:349–355
45. Sadeghzadeh SM (2015) RSC Adv 5:68947–68952
46. Fan L, Wang J, Zhang X, Sadeghzadeh SM, Zhiani R, Shahroudi M, Amarloo F (2019) Catal Lett 149:3465–3475
47. Sadeghzadeh SM, Zhiani R, Emrani S (2017) RSC Adv 7:24885–24894
48. Maleki A, Hajizadeh Z, Abbasi H (2018) Carbon Lett 27:42
49. Maleki A, Paydar R (2015) RSC Adv 5:33177–33184
50. Maleki A, Rahimi J (2018) J Porous Mater 25:1789–1796
51. Shahabi Nejad M, Seyedi N, Sheibani H (2019) Mater Chem Phys 238:121849
52. Shahabi Nejad M, Behzadi S, Sheibani H (2019) Appl Organomet Chem e5166
53. Esmaeili N, Mohammadi P, Abbaszadeh M, Sheibani H (2019) Int J Hydrog Energy 44:23002–23009
54. Le Normand F, Hommet J, Szörényi T, Fuchs C, Fogarassy E (2001) Phys Rev B 64:235416
55. Cao LM, Zhang XY, Gao CX, Wang WK, Zhang ZL, Zhang Z (2003) Nanotechnology 14:931–934
56. Machnikowski J, Grzyb B, Weber JV, Frackowiak E, Rouzaud JN, Béguin F (2004) Electrochim Acta 49:423–432